

# Identification of a *KEAP1* Germline Mutation in a Family with Multinodular Goitre

Risa Teshiba<sup>1,5</sup>, Tatsuro Tajiri<sup>2</sup>, Kenzo Sumitomo<sup>3</sup>, Kouji Masumoto<sup>4</sup>, Tomoaki Taguchi<sup>5</sup>, Ken Yamamoto<sup>1\*</sup>

**1** Division of Genome Analysis, Research Center for Genetic Information, Medical Institute of Bioregulation, Kyushu University, Fukuoka, Japan, **2** Department of Pediatric Surgery, Graduate School of Medical Sciences, Kyoto Prefectural University of Medicine, Kyoto, Japan, **3** Department of Pediatric Surgery, Shimonoseki City Hospital, Shimonoseki, Japan, **4** Department of Pediatric Surgery, Faculty of Medicine, University of Tsukuba, Tsukuba, Japan, **5** Department of Pediatric Surgery, Reproductive and Developmental Medicine, Graduate School of Medical Sciences, Kyushu University, Fukuoka, Japan

## Abstract

**Background:** The familial clustering of multinodular goitres (MNGs) with a dominant mode of inheritance has been repeatedly reported. Linkage studies have revealed several genetic loci responsible for familial MNG; however, most of the causative variants remain unknown.

**Methods and Results:** Through linkage analysis using single-nucleotide polymorphism markers, we identified a new MNG locus on 19p13.2-q12 in a five-generation Japanese MNG family. Subsequent mutation searches focusing on the candidate 25-Mb region of chromosome 19 identified a heterozygous mutation, c.879\_880delinsA, p.Asp294Thr, fs\*23, in exon 3 of the *KEAP1*, which plays a central role in the cytoprotection pathway against oxidative stress. Reverse transcriptase-PCR analysis showed low expression of wild type *KEAP1* accompanied by no transcription product of mutant allele in the normal and goitre region of thyroid tissues obtained from the proband. In agreement with previous studies showing that *KEAP1* negatively regulates NFE2L2, the NFE2L2 target genes *GSTA4* and *GCLC* were up-regulated in the thyroid tissues of the patient.

**Conclusions:** This study identified the first *KEAP1* mutation in MNG. The results provide insights into the pathogenesis of goitre which develops in the organ continuously exposed to oxidative stress during hormone synthesis.

**Citation:** Teshiba R, Tajiri T, Sumitomo K, Masumoto K, Taguchi T, et al. (2013) Identification of a *KEAP1* Germline Mutation in a Family with Multinodular Goitre. PLoS ONE 8(5): e65141. doi:10.1371/journal.pone.0065141

**Editor:** Maurice A.M. van Steensel, Maastricht University Medical Center, The Netherlands

**Received:** December 18, 2012; **Accepted:** April 22, 2013; **Published:** May 28, 2013

**Copyright:** © 2013 Teshiba et al. This is an open-access article distributed under the terms of the Creative Commons Attribution License, which permits unrestricted use, distribution, and reproduction in any medium, provided the original author and source are credited.

**Funding:** This work was supported by the grant (No.22133003) from the Ministry of Education, Culture, Sports, Science and Technology of Japan. The funders had no role in study design, data collection and analysis, decision to publish, or preparation of the manuscript.

**Competing Interests:** The authors have declared that no competing interests exist.

\* E-mail: kyama@bioreg.kyushu-u.ac.jp

## Introduction

A nontoxic multinodular goitre (MNG) (Online Mendelian Inheritance in Man [OMIM] 138800) is clinically characterised by the nodular enlargement of the thyroid gland without thyroid dysfunction or inflammation. In general population in an area with borderline iodine deficiency, MNG are found by ultrasonography in approximate 23% of the population [1]. Multiple factors, such as sex, iodine deficiency and smoking, influence the development of MNG [2–5]. In addition, familial and twin studies in endemic and nonendemic regions have indicated a genetic predisposition for MNGs [2,5–7]. Because a history of MNG has been suggested to be a risk factor for the development of toxic goitres and thyroid cancer [8,9], it is important to identify the genes involved in MNG for early diagnosis and for a better understanding of the pathogenesis of thyroid disease.

Linkage analysis using familial MNG has been one of the approaches used to identify causative genes for the disease. Several studies have reported genetically linked loci for familial MNG. Studies in German and Canadian pedigrees with nontoxic MNG identified a susceptibility locus on chromosome 14q, which is

called MNG-1 (OMIM 138800) [10,11]. In 2000, Capon et al. mapped MNG-2 (OMIM 300273) on chromosome Xp22 with linkage analysis of a three-generation Italian pedigree [12]. Another locus, MNG-3 (OMIM 606082), was identified on chromosome 3q26.1-q26.3 from two independent Japanese pedigrees presenting with MNG with euthyroidism and high thyroid-stimulating hormone levels [13]. Furthermore, four candidate loci were reported on chromosomes 2q, 3p, 7q and 8p with linkage analysis in Danish, German and Slovakian families [14]. Thus, linkage results indicate genetic heterogeneity in the aetiology of MNG, even in familial cases with a Mendelian mode of inheritance [15].

Based on observations that pleuropulmonary blastoma (PPB) families also have MNG, Rio Frio et al. screened mutations of the PPB-causative gene *dicer 1*, ribonuclease type III (*DICER1*), which is located in the MNG-1 locus in MNG families, and identified several mutations linked to MNG [16]. However, except for this recent finding, causative genes for euthyroid MNG in other loci have remained unclear. Considering the genetic heterogeneity of the disease, additional linkage analyses using additional families to validate reported loci or to detect novel loci followed by

comprehensive sequencing analysis targeting linkage regions are required to explain the genetic aetiology of MNG.

In the present study, we identified a novel germline mutation in kelch-like ECH-associated protein 1 (*KEAP1*) in a Japanese pedigree with MNG through a combination of genome-wide linkage analysis using a high-density single-polymorphism nucleotide (SNP) array and next-generation sequencing. Subsequent gene expression analysis showed the functional activation of nuclear factor (erythroid-derived 2)-like 2 (*NFE2L2*), which is negatively regulated by *KEAP1*, in the thyroid tissue of the patient. Our study suggests that dysfunction of the *KEAP1*-*NFE2L2* stress-response pathway may contribute to the nodular process in thyroid tissue, which is physiologically exposed to the oxidative nature of thyroid hormone synthesis.

## Methods

### Subjects

We identified a 5-generation Japanese family presenting with a dominant inheritance pattern of familial thyroid goitre (Figure 1 and Table S1). The proband (V:2) was a 15-year-old girl from the western area of Japan who had been referred to our hospital. Ultrasonographic examination showed multiple cystic lesions in both of the thyroid lobes, and the level of thyroid hormone was within the normal range (TSH, 0.67  $\mu$ U/ml; free T3, 4.16 pg/ml; free T4, 1.56 ng/dl). Her older sister (V:1) had a thyroid lobectomy at 8 years old. Their pathological diagnoses were adenomatous goitre. They do not show any sign of malignancy in organs including the thyroid in medical follow-up after a thyroid lobectomy. We obtained 13 blood samples from the family, including 8 affected (III:4, III:6, III:8, IV:2, IV:4, V:1, V:2 and V:4) and 5 unaffected (III:3, III:9, IV:1, IV:3 and V:3) individuals, and goitre and matched normal thyroid tissue from the proband (V:2). The age of onset was 8–50 years old. None of the affected individual showed any evidence of malignancy. A total of 192 unrelated normal controls from a population-based Japanese cohort were subjected to sequencing to evaluate the frequency of the *KEAP1* mutation in the general population. All participants provided their written informed consent to participate in this study according to the Declaration of Helsinki. We obtained written informed consent from the parents on the behalf of the children participants. This study was approved by the Ethics Committee at Kyushu University, Fukuoka, Japan.

### DNA isolation and SNP genotyping

Genomic DNA was extracted from peripheral blood leukocytes using the QIAamp DNA Blood Midi Kit (Qiagen) and adjusted to a final concentration of 50 ng/ $\mu$ l for SNP typing. The Illumina Human CNV370K-Quad Array and the Illumina BeadStation 500G SNP genotyping system were employed for genome-wide SNP typing according to the manufacturer's protocols. SNP genotypes were determined with the BeadStudio Genotyping Analysis Module 3.3.7 software. All of the samples showed call rates greater than 0.99 (the average was 0.998, Table S2), and 342,115 SNPs on chromosomes 1 to X had a call frequency of 1.0. Based on the results of the Mendelian error check of PLINK v1.06 (<http://pngu.mgh.harvard.edu/purcell/plink/>) [17], 293 SNPs were excluded, and the remaining 341,822 SNPs were available for linkage analysis. To estimate genome-wide pairwise IBD, we additionally excluded 94,826 SNPs that were homozygous in all of the samples; the remaining 246,996 SNPs were subjected to the IBD analysis. The quality control of the SNP typing is shown in Figure S1.

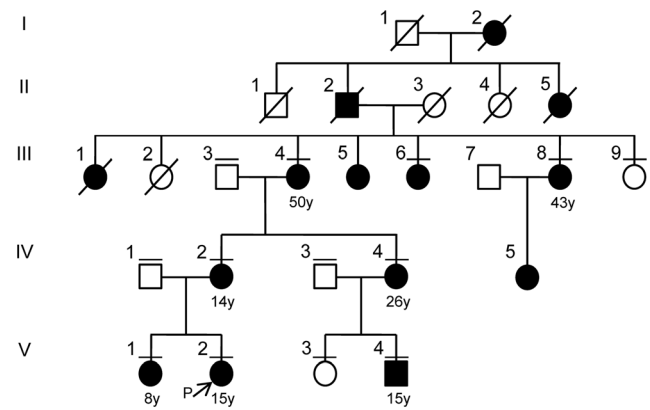


**Figure 1. A pedigree of a five-generation multinodular goitre family.** Individuals are numbered above each symbol. Individuals affected with MNG are indicated by filled symbols and age of onset is described under the patient symbol. The arrow shows a proband of this family study. The bars above each symbol indicate individuals included in the linkage analysis.  
doi:10.1371/journal.pone.0065141.g001

### Statistical analysis

The genome-wide IBD for all pairs of individuals was estimated using PLINK v1.06 to evaluate pedigree errors. Multipoint parametric LOD scores and the information score were calculated using GeneHunter v2.1r5 (with easyLINKAGEPlus v5.08) [18,19]. A total of 3,514 and 454 SNPs whose pair-wise *r*-square was  $<0.01$  were automatically selected by easyLINKAGE for linkage analysis to the whole genome (1.0 cM spacing) and to chromosome 19 (0.2 cM spacing), respectively (Table S3). The model used in the parametric analyses assumed a dominant model of inheritance, a disease allele frequency of 0.001 and complete penetrance. The marker genetic position was based on the Marshfield linkage map [20], and the sex-averaged position was applied.

### Exome capture and next-generation sequencing

The genomic DNA of the proband was subjected to sequencing. The SureSelect Human All Exon System (Agilent Technologies) was employed to capture whole-genome exons. The Illumina Genome Analyser GAIIx was used for sequencing, and 75 base reads were generated.

### Read mapping and variant analysis of the linkage region

Read mapping and the subsequent variant analysis of chromosome 19 were performed with CLC Genomic Workbench 4.6.1 (CLC bio). The following parameters were used to map reads to a reference genome (GRCh37): similarity = 0.95, length fraction = 1.0, insertion cost = 3, deletion cost = 3 and mismatch cost = 2. Subsequently, to discover the conflict of a mapping, SNP and DIP (deletion/insertion polymorphisms) detections were performed using the default setting. To select potential mutations critical for the pathology of MNG, we eliminated the known variants that were listed in dbSNP132 or the variants that showed synonymous amino acid substitution. The reads that were incorrectly mapped were identified and removed using BLAT Search Genome in the UCSC database (<http://genome.ucsc.edu/>). The conflicts that resulted in a low quality value were considered to be artefacts. A summary of the sequencing and mapping is shown in Figure S2. Polyphen-2, Mutation Taster and SIFT classification tools were used to determine the amino acid changes that most likely destroyed protein function [21–23]. The direct sequencing of

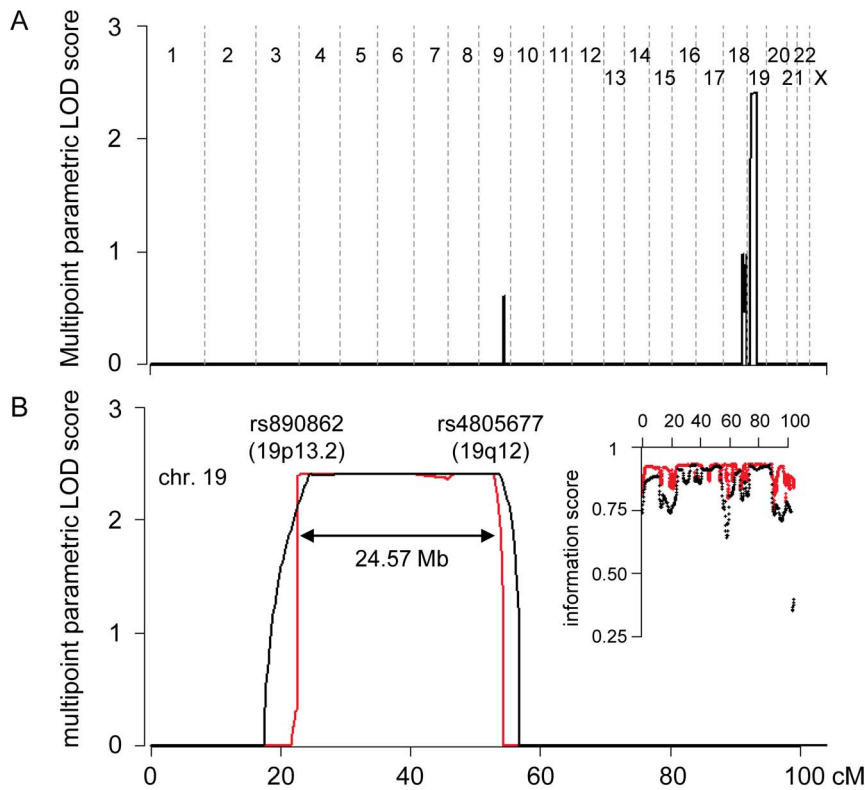


**Figure 2. Summary of the genome-wide SNP linkage analysis.** (A) The multipoint parametric LOD (pLOD) score with a marker interval of 1.0 cM is shown for all of the autosomes and the X chromosome. (B) The multipoint pLOD and the information score of chromosome 19 are shown. The black and red lines (or dot) denote results from 1.0 and 0.2 cM marker interval analysis, respectively. doi:10.1371/journal.pone.0065141.g002

*KEAP1* was performed using the primers 5'-CTGAGC-GACTGTGCGGAAGTA-3' and 5'-GGCCAAGCAAGAGGAG-TTCT-3' for PCR amplification and the primer 5'-GGCCAAG-CAAGAGGAGTTCT-3' (the reverse primer of PCR) for sequencing according to a standard procedure.

#### Reverse transcriptase-PCR

Total RNA was extracted from frozen thyroid tissues of the proband using an RNeasy Mini Kit (Qiagen) and was subjected to reverse transcription with the use of a First-strand cDNA Synthesis Kit (GE Healthcare). The resulting cDNA was then subjected to PCR analysis using 4 primer pairs: *KEAP1*-N-fwd, 5'-CCTGCAGTGACTTCCTGGTG-3' (forward); *KEAP1*-N-rvs, 5'-GTGGAAGACCTCGGACTCG-3' (reverse); *KEAP1*-C-fwd, 5'-ATGAGCGTGCCCCGTAAC-3' (forward); *KEAP1*-C-rvs, 5'-CACGGCATAAAGGAGACGAT-3' (reverse); *KEAP1*-mut-fwd, 5'-CATCTACATGCATTTTGGGGAG-3' (forward); *KEAP1*-mut-rvs, 5'-TAGTCCTTGACGCGGGAGTT-3' (reverse); *GAPDH*-fwd, 5'-ACCACAGTCCATGCCATCAC-3' (forward); *GAPDH*-rvs, 5'-TCCACCACCCTGTTGCTGTA-3' (reverse). The *KEAP1*-mut-rev primer contained the "T" nucleotide at the 3' end to achieve specific amplification of mutated allele. The wild type full-length *KEAP1* cDNA and truncated *KEAP1* cDNA containing c.879\_880delinsA mutation were cloned into *SfiI* and *XhoI* sites of pCMV-myc plasmid (Life Technologies) for the control templates of PCR.

#### Real-time PCR

The cDNA generated as mentioned above was also subjected to real-time PCR analysis in triplicate for evaluation of the expression

of *NFE2L2* and its target genes glutathione S-transferase alpha 4 (*GSTA4*), glutamate-cysteine ligase catalytic subunit (*GCLC*) and NAD(P)H dehydrogenase quinone 1 (*NQO1*) with the use of a TaqMan Gene Expression Assay (Life Technologies) and the On ECO Real-time PCR System (Illumina), with glyceraldehyde-3-phosphate dehydrogenase (*GAPDH*) cDNA serving as an endogenous control. The following TaqMan probes were used: *NFE2L2* (Hs00232352\_m1), *GSTA4* (Hs00155308\_m1), *GCLC* (Hs00155249\_m1) and *NQO1* (Hs00168547\_m1). The amount of mRNA was calculated by the comparative CT method [24], and all data were normalized by the amount of *GAPDH* mRNA.

#### Results

Genome-wide SNP typing enables the estimation of pairwise identity-by-descent (IBD) to examine the relationships of family members. Because pedigree error leads to incorrect results for linkage analysis, we first calculated the pairwise proportions of IBD in all of the samples and compared them with the theoretical values obtained from the pedigree chart. The genetic relationship of all of the pairs was consistent with the clinically obtained family relationship data (Figure S3); thus, linkage analysis was performed based on the original pedigree.

The results of the multipoint linkage analyses using SNP markers are shown in Figure 2. A maximum parametric LOD (pLOD) score of 2.41 was obtained on chromosome 19, spanning approximately 25 Mb between rs890862 and rs4805677. The information scores approached 0.9 as the interval of the markers became narrower (Figure 2B), suggesting that analysis with a 0.2 cM marker interval was a more powerful test than a 1.0 cM

**Table 1.** Novel variants identified in the proband in the chromosome 19 linkage region.

Algorithm	Position of ref. on Chr19	Gene	Ref. base	Variant base	Count (ref./variant)	Frequency (ref./variant)	Amino acid change	Mutation taster	PolyPhen-2 v2.1.0		SIFT
									HumVar	evaluation	
DIP detection	10,602,698	KEAP1	C	-	27/28	49.1/50.9	frameshift	Disease causing	-	-	-
SNP detection	8,196,653	FBN3	C	T	0/11	0/100	Gly592Asp	Disease causing	1.000	Most likely damaging	Not scored
	9,068,277	MUC16	G	C	17/12	58.6/41.4	Ala6390Gly	Polymorphism	NA	Not predicted	Not predicted
	10,445,269	ICAM3	C	T	44/56	44.0/56.0	Ser376Asn	Polymorphism	0.006	Benign	Not scored
	11,943,552	ZNF440	G	A	101/97	51.0/49.0	Gly521Arg	Polymorphism	0.012	Benign	Tolerated
	16,613,993	C19orf44	C	T	76/77	49.7/50.3	Arg293Cys	NA	0.098	Benign	Tolerated
	21,239,988	ZNF430	G	A	159/151	51.3/48.7	Glu291Lys	Polymorphism	0.045	Benign	Tolerated

ref.: reference sequence.  
doi:10.1371/journal.pone.0065141.t001

interval. Linkage signals for the previously reported loci, MNG-1, -2 and -3 and chromosomes 2q, 3p, 7q and 8p, were almost zero (Figure 2A). The linkage analysis suggested that 19p13.2-q12 is a causative region in this family.

Three candidate genes were present within this linkage region: translocase of inner mitochondrial membrane 44 (*TIMM44*), NADH dehydrogenase (ubiquinone) 1 alpha subcomplex, 13 (*NDUFA13*) and solute carrier family 5 (sodium iodide symporter), member 5 (*SLC5A5*). Mutations in *TIMM44* and *NDUFA13* have been reported to be associated with tumorigenesis in the thyroid [25,26], and the *SLC5A5* gene encodes sodium-iodide symporter protein, whose down-regulation is associated with thyroid carcinomas [27]. However, no mutation was identified in these genes in our samples (data not shown).

Considering the broad range of the linkage region, in which approximately 660 genes reside, we applied a next-generation sequencing technique for the identification of the causative mutation of MNG. The genomic DNA from a proband was subjected to exon capture, and a total of 263,794,206 reads with 75 bases were obtained with sequencing. A total of 5,314,723 reads were mapped to the reference sequence of chromosome 19 using *CLC* Genomics Workbench. The mean depth of coverage for the coding sequences was 92.1x, and 88.9% of the coding sequences on chromosome 19 were covered at greater than or equal to 1x depth. Within the exons and exon-intron boundaries of the linkage region, 7,222 single-nucleotide variations and 419 small deletions/insertions were detected with the SNP and DIP detection algorithms, respectively. After removing known variants, synonymous substitutions, systematic artefacts and coverage <10x, seven variants remained (Table 1 and Figure S2).

The six missense variants and one deletion were evaluated to determine functionally significant changes using Mutant Taster (<http://www.mutationtaster.org/>), PolyPhen-2 (<http://genetics.bwh.harvard.edu/pph2/>) and SIFT (<http://sift.bii.a-star.edu.sg/>) programs [21–23]. Four variants located in *ICAM3*, *ZNF440*, *C19orf44* or *ZNF430* were assumed to lead to non-hazardous changes in protein function because at least two programs evaluated them as "polymorphism", "benign" or "tolerated" (Table 1). Indeed, the variants in *ICAM3*, *ZNF440* or *C19orf44* were recently identified by 1000 Genome Project (rs117942573, rs117998813 or rs199764040, respectively). Therefore, we excluded these four variants from further analysis. A variant in *MUC16* was evaluated as "polymorphism" by the Mutation Taster program, and expression of this gene in the thyroid was suggested to be considerably low based on several databases including BioGPS (<http://biogps.org/>), Cancer Genome Anatomy Project (<http://cgap.nci.nih.gov/SAGE>) and GeneHub-GEPIs (<http://research-public.gene.com/Research/genentech/genehub-gepis/>). These results suggested that the variant in *MUC16* could not be a significant candidate of causative mutation of the MNG. Regarding a variant in *FBN3*, all of the read contained the variant base, indicating that the genotype was homozygous for the variant. Therefore, it was unlikely that this variant causes the disease with dominant mode of inheritance. Finally, we selected a frame shift variant in *KEAP1* for further analysis because it was a novel variant, evaluated as "disease causing", and showed heterozygous genotype.

Direct sequencing of the *KEAP1* variant in the proband identified a frameshift mutation in exon 3 of the gene: c.879\_880delinsA, p.Asp294Thr, fs\*23 (Figure 3A). The subsequent sequencing of family members confirmed the co-segregation of the mutation in affected individuals (Figure S4). However, the mutation was not observed in 192 Japanese normal control samples.

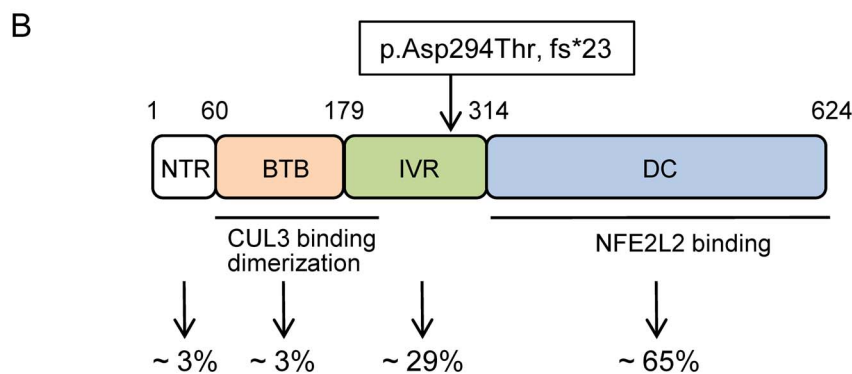
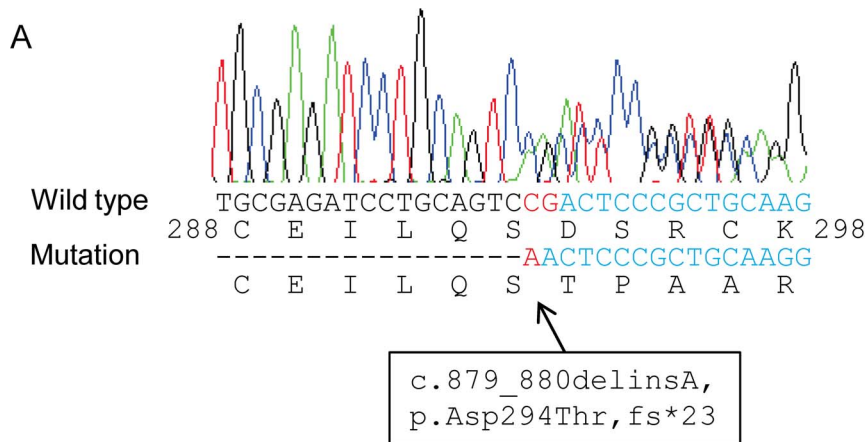


**Figure 3. Identification of a heterozygous mutation in *KEAP1*.** (A) The result of Sanger sequencing of proband DNA showed the c.879\_880delinsA mutation (red), resulting in a 1-base deletion and a frameshift (p.Asp294Thr, fs\*23) in *KEAP1*. (B) Domain structure and mutation location in the *KEAP1* protein. The protein consists of an N-terminal region (NTR; amino acids 1 to 60), a BTB domain (amino acids 61 to 179), an intervening region (IVR; amino acids 180 to 314) and a DC domain (amino acids 315 to 624). The BTB and N-terminal portion of IVR is responsible for dimerisation and the interaction with CUL3. The DC domain is also critical for the interaction with NFE2L2. The p.Asp294Thr, fs\*23 mutation is located in the IVR. The reported frequencies of the somatic mutations observed in each domain in cancer cells are shown at the bottom [32]. doi:10.1371/journal.pone.0065141.g003

*KEAP1* is a cytoplasmic protein that acts as a negative regulator of NFE2L2 [28–30]. *KEAP1* interacts with NFE2L2 via an DC domain comprising six Kelch repeats and a C-terminal region and also associates with CUL3 via a broad complex tramtrack bric-a-brac (BTB) homodimerisation domain to form an E3 ubiquitin ligase complex, resulting in the constitutive degradation of NFE2L2 (Figure 3B). Somatic mutations that impair the function of *KEAP1* and lead to the constitutive stabilisation of NFE2L2 have been found in lung, gallbladder and liver cancer in humans (Figure 3B) [31,32]. Because the p.Asp294Thr, fs\*23 mutation identified in this study resides in a DC domain, we questioned whether this mutation could generate a truncated *KEAP1* protein or not. We examined the expression of the mutant *KEAP1* in the thyroid tissues of the patient by reverse transcriptase-PCR using 3 primer pairs (Fig 4A). We designed a primer pair (*KEAP1*-mut-fwd and *KEAP1*-mut-rvs) that specifically amplifies mutant *KEAP1* and 2 primer pairs that amplify 5' or 3' portion flanking the mutation of *KEAP1* (*KEAP1*-N-fwd and *KEAP1*-N-rvs, or *KEAP1*-C-fwd and *KEAP1*-C-rvs, respectively). It was found that expression of the c.879\_880delinsA mutant was almost nil in the thyroid tissues of the patient as well as in the normal thyroid (Fig 4B, upper panel). On the other hand, expression of the 5' and 3' portion of *KEAP1* were observed in the thyroid of patient; however, the expression level was lower in the tissues of patient

than normal thyroid (Fig. 4B, second and third panels). These results suggested that truncated *KEAP1* protein is not generated probably due to non-sense mediated mRNA decay, and that the expression of wild type *KEAP1* protein might be decreased due to low transcription product, at least in the thyroid tissues of the patient.

To investigate the effect of decreased expression of *KEAP1*, we performed qPCR analysis for the NFE2L2 target genes, *GCLC*, *GSTA4* and *NQO1*. As shown in Figure 5, the expression of *GCLC* and *GSTA4* were significantly elevated in both the normal and goitre portion of the thyroid tissue obtained from the proband compared with control thyroid RNA. Regarding *NQO1*, an increasing trend was detected, but this increase was not statistically significant. The expression of *NFE2L2* was not changed, consistent with the theory that *KEAP1* affects NFE2L2 localisation but not expression. The results suggested that the decreased expression of *KEAP1* might result in activation of NFE2L2 target genes, at least in the thyroid of the patients.

## Discussion

The thyroid gland maintains its homeostasis in the face of an increased burden of free radicals and reactive oxygen species produced during iodine metabolism for thyroid hormone synthe-

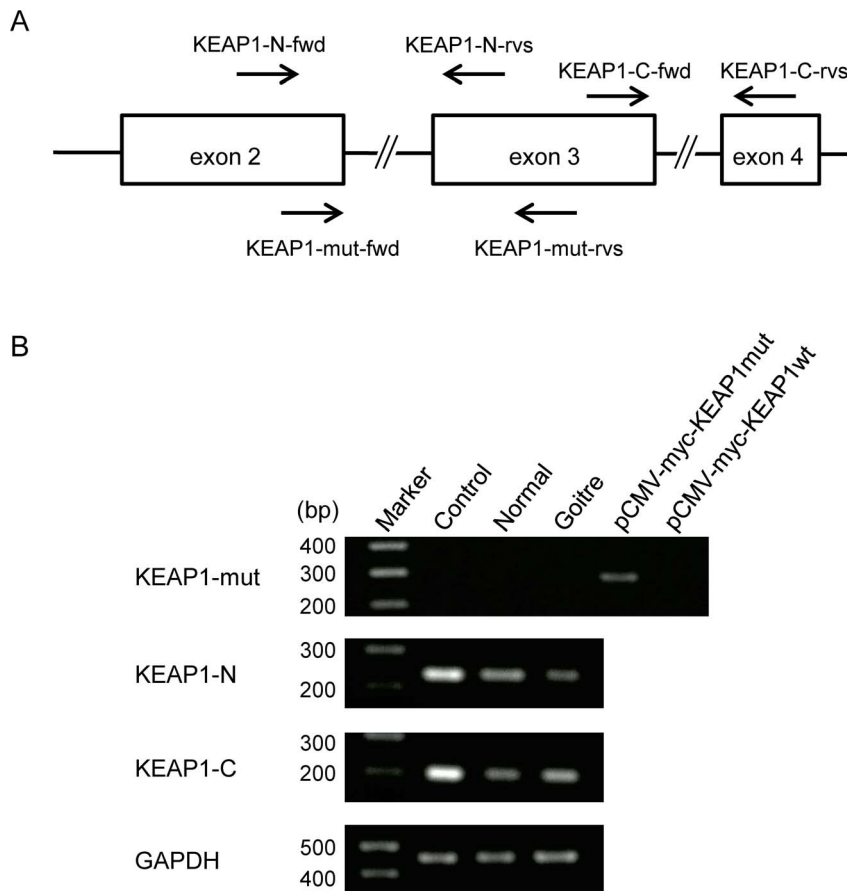


**Figure 4. Reverse transcriptase-PCR for mutant and wild type *KEAP1*.** (A) Primer positions for reverse transcriptase-PCR in *KEAP1* exons. The asterisk indicates the position of c.879\_880delinsA mutation in exon 3. The primer, KEAP1-mut-rvs, contains "T" nucleotide at the 3' end which is the complement of mutant "A" nucleotide to amplify mutant allele. The expected sizes of PCR products are as follows: 233 bp for KEAP1-N-fwd and KEAP1-N-rvs; 201 bp for KEAP1-C-fwd and KEAP1-C-rvs; 282 bp for KEAP1-mut-fwd and KEAP1-mut-rvs. (B) Results of the reverse transcriptase-PCR for the mutant and wild type *KEAP1*. cDNAs from control normal thyroid, the normal and goitre region of thyroid tissues obtained from the proband were amplified by 3 primer sets indicated in (A) to mutant *KEAP1* (upper panel), 5' and 3' normal portions adjacent mutation site (second and third panels, respectively) of *KEAP1*. *GAPDH* was amplified as a control for the amount of cDNA in each sample. The expected size of PCR product of *GAPDH* is 452 bp. In the experiment of mutant *KEAP1* amplification, the plasmids containing mutant or wild type *KEAP1* (pCMV-myc-*KEAP1*mut or pCMV-myc-*KEAP1*wt, respectively) were utilized as control templates. doi:10.1371/journal.pone.0065141.g004

sis. When the gland is exposed to additional oxidative stress caused by smoking and iodine deficiency, it is assumed that the excessive damage of lipids, proteins and DNA leads to thyroid dysfunction, including goitre formation. Indeed, these environmental factors are well known risk factors for MNG. Therefore, the genes involved in the signal cascades protecting cellular homeostasis against oxidative stress would be candidates for the genetic aetiology of MNG.

The KEAP1-NFE2L2 regulatory pathway is a major biological defence system against oxidative damage [32,33]. In response to oxidative and electrophilic stress, key cysteine residues of KEAP1 are oxidised to allow NFE2L2 to dissociate from the ubiquitination activity of the complex. NFE2L2 subsequently translocates into the nucleus and transactivates a series of cytoprotective genes, including *NQO1*, *GCLC* and *GST*. Notably, somatic mutations that stabilise NFE2L2, thus conferring protection against oxidative stress, have been identified in *KEAP1* in human cancers [32]. To our knowledge, however, germline mutation in *KEAP1* has not been described in familial cancer cases. A recent study suggested that the NFE2L2-mediated adaptation to oxidative stress is crucial for the early stages of tumour development [34]. In this study, we

observed that the expression of NFE2L2 target genes were increased accompanied by decreased expression of wild type *KEAP1* in the thyroid tissues obtained from the proband. This suggests that the KEAP1-NFE2L2 pathway might be impaired in the tissues of the patient with the heterozygous c.879\_880delinsA mutation, supporting that this MNG family showed dominant mode of inheritance.

The mechanisms through which the patients in the present study were affected with only MNG are unclear. One possibility is that the thyroid gland is most susceptible to additional oxidative stress, in other words, dysregulated NFE2L2 activation, because this gland is physiologically and continuously exposed to stress during hormone synthesis. It is also possible that tumours developed in multiple organs but were not clinically detected due to insufficient examination. An intensive follow-up of the course of the patients would be required for the early diagnosis of tumours in different organs.

Several linkage loci in addition to chromosome 19 have been detected for familial MNG; therefore, it cannot be concluded that the *KEAP1* is the major causative gene of familial cases. Indeed, this is the first report of *KEAP1* mutation in thyroid diseases.

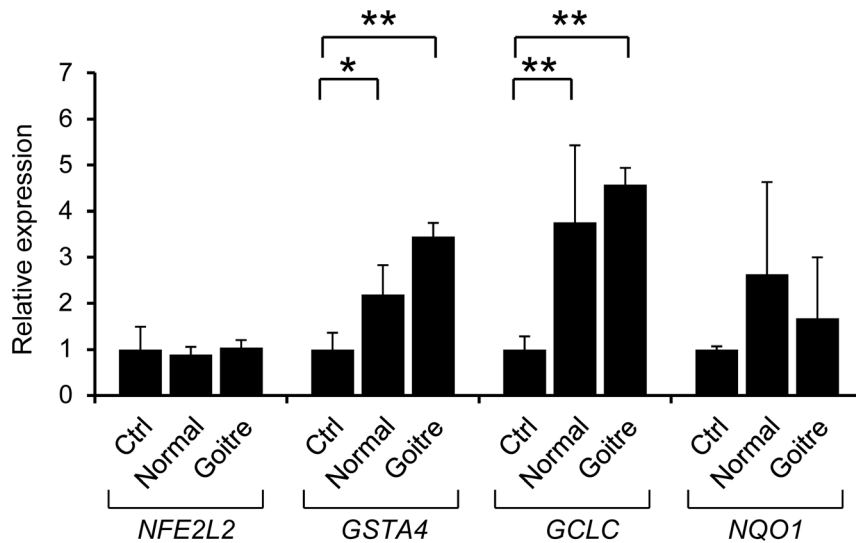


**Figure 5. Up-regulation of NFE2L2 target genes in the thyroid tissues of the patient.** Results of the quantitative PCR of *NFE2L2* and its target genes *GSTA4*, *GCLC* and *NQO1* in the normal and goitre region of thyroid tissues obtained from the proband. The expression levels relative to control RNA from an adult thyroid are shown. The significance with the t-test is indicated with asterisks (\* $p < 0.05$  and \*\* $p < 0.01$ ). doi:10.1371/journal.pone.0065141.g005

However, the association of common variants of *KEAP1* and *NFE2L2* with sporadic cases of MNG should be considered.

In summary, we identified a new MNG locus on chromosome 19p13.2-q12 through linkage analysis using high-density SNP markers. Subsequent sequence analysis focused on the linkage region revealed a heterozygous mutation of c.879\_880delinsA, p.Asp294Thr, fs\*23 in *KEAP1*, which plays a central role in cell protection against oxidative stress. In agreement with the molecular function of KEAP1, the NFE2L2 target genes *GSTA4* and *GCLC* were up-regulated in the thyroid tissues of the patient, which may be caused by low expression of wild type *KEAP1*. The present study implies that a functional defect of genes involved in maintaining the homeostasis against the oxidative stress physiologically generated during thyroid hormone synthesis could cause tumorigenesis in this organ.

## Supporting Information

**Figure S1 Genotype quality check of SNPs for the genome-wide linkage analysis.** (TIFF)

**Figure S2 Summary of sequencing and read mapping.** (TIFF)

**Figure S3 Results of the estimated proportions of IBD.** The degree of relatedness for each pair is described to the left of the diagonal (UR: unrelated), and the pairwise proportion of IBD calculated by PLINK is shown to the right of the diagonal. The red, pink, blue and white cells in the proportions of IBD indicate 1st-, 2nd- and 3rd-degree relatives and unrelated pairs, respectively.

## References

- Knudsen N, Perrild H, Christiansen E, Rasmussen S, Dige-Petersen H, et al. (2000) Thyroid structure and size and two-year follow-up of solitary cold thyroid nodules in an unselected population with borderline iodine deficiency. *Eur J Endocrinol* 142: 224–230.
- Krohn K, Führer D, Bayer Y, Eszlinger M, Brauer V, et al. (2005) Molecular pathogenesis of euthyroid and toxic multinodular goiter. *Endocr Rev* 26: 504–524.
- Hegedüs L, Bonnema SJ, Bennedbaek FN. (2003) Management of simple nodular goiter: Current status and future perspectives. *Endocr Rev* 24: 102–132.
- Laurberg P, Jørgensen T, Perrild H, Ovesen L, Knudsen N, et al. (2006) The Danish investigation on iodine intake and thyroid disease. *Eur J Endocrinol* 155: 219–228.
- Brix TH, Hegedüs L. (2000) Genetic and environmental factors in the aetiology of simple goiter. *Ann Med* 32: 153–156.
- Greig WR, Boyle JA, Duncan A, Nicol J, Gray MJ, et al. (1967) Genetic and non-genetic factors in simple goitre formation: evidence from a twin study. *Q J Med* 142: 175–188.

tively. The results indicated that the proportions of IBD are consistent with the clinically obtained pedigree chart. (TIFF)

**Figure S4 Co-segregation of the KEAP1 mutation in a multinodular goitre family.** WT/WT: homozygous for wild-type KEAP1, WT/mut: heterozygous for the KEAP1 c.879\_880delinsA mutation. (TIFF)

**Table S1 Clinical features of the patients.** (DOCX)

**Table S2 Call rate of each sample in the genotyping using Illumina Human CNV370K-Quad Array.** (DOCX)

**Table S3 Number of SNPs on each chromosome analyzed in the multipoint linkage analysis using Genehunter v2.1r5 program.** (DOCX)

## Acknowledgments

We thank all of the patients and family members who participated in this study. We would also like to thank T. Akinaga, M. Sonoda and K. Fukuyama for their technical services.

## Author Contributions

Conceived and designed the experiments: RT KM KY. Performed the experiments: RT KY. Analyzed the data: RT KY. Contributed reagents/materials/analysis tools: TT KS TT. Wrote the paper: RT KY.

7. Bayoumi RA, Taha TS, Saha N. (1988) Study of possible genetic predisposition to endemic goitre among the Fur and Baggara tribes of the Sudan. *Hum Hered* 38: 8–11.
8. Ngan ES, Lang BH, Liu T, Shum CK, So MT, et al. (2009) A germline mutation (A339V) in thyroid transcription factor-1 (TTF-1/NKX2.1) in patients with multinodular goiter and papillary thyroid carcinoma. *J Natl Cancer Inst* 101: 162–175.
9. Arora N, Scognamiglio T, Zhu B, Fahey TJ 3rd. (2008) Do benign thyroid nodules have malignant potential? An evidence-based review. *World J Surg* 32: 1237–1246.
10. Bignell GR, Canzian F, Shayeghi M, Stark M, Shugart YY, et al. (1997) Familial Nontoxic multinodular thyroid goiter locus maps to chromosome 14q but does not account for familial nonmedullary thyroid cancer. *Am J Hum Genet* 61: 1123–1130.
11. Neumann S, Willgerodt H, Ackermann F, Reske A, Jung M, et al. (1999) Linkage of familial euthyroid goiter to the multinodular goiter-1 locus and exclusion of the candidate genes thyroglobulin, thyroperoxidase, and  $\text{Na}^+/\text{I}^-$  symporter. *J Clin Endocrinol Metab* 84: 3750–3756.
12. Capon F, Tacconelli A, Giardina E, Sciacchitano S, Bruno R, et al. (2000) Mapping a dominant form of multinodular goiter to chromosome Xp22. *Am J Hum Genet* 67: 1004–1007.
13. Takahashi T, Nozaki J, Komatsu M, Wada Y, Utsunomiya M, et al. (2001) A new locus for a dominant form of multinodular goiter on 3q26.1-q26.3. *Biochem Biophys Res Commun* 284: 650–654.
14. Bayer Y, Neumann S, Meyer B, Rüschemdorf F, Reske A, et al. (2004) Genome-wide linkage analysis reveals evidence for four new susceptibility loci for familial euthyroid goiter. *J Clin Endocrinol Metab* 89: 4044–4052.
15. Neumann S, Bayer Y, Reske A, Tajtáková M, Langer P, et al. (2003) Further indications for genetic heterogeneity of euthyroid familial goiter. *J Mol Med* 81: 736–745.
16. Rio Frio T, Bahubeshi A, Kanellopoulou C, Hamel N, Niedziela M, et al. (2011) DICER1 mutations in familial multinodular goiter with and without ovarian Sertoli-Leydig cell tumors. *JAMA* 305: 68–77.
17. Purcell S, Neale B, Todd-Brown K, Thomas L, Ferreira MA, et al. (2007) PLINK: a tool set for whole-genome association and population-based linkage analyses. *Am J Hum Genet* 81: 559–575.
18. Kruglyak L, Daly MJ, Reeve-Daly MP, Lander ES. (1996) Parametric and nonparametric linkage analysis: a unified multipoint approach. *Am J Hum Genet* 58: 1347–1363.
19. Hoffmann K, Lindner TH. (2005) easyLINKAGE Plus – Automated linkage analyses using large-scale SNP data. *Bioinformatics* 21: 3565–3567.
20. Broman KW, Murray JC, Sheffield VC, White RL, Weber JL. (1998) Comprehensive human genetic maps: Individual and sex-specific variation in recombination. *Am J Hum Genet* 63: 861–869.
21. Schwarz JM, Rödelberger C, Schuelke M, Seelow D. (2010) MutationTaster evaluates disease-causing potential of sequence alterations. *Nat Methods* 7: 575–576.
22. Adzhubei IA, Schmidt S, Peshkin L, Ramensky VE, Gerasimova A, et al. (2010) A method and server for predicting damaging missense mutations. *Nat Methods* 7: 248–249.
23. Ng PC, Henikoff S. (2003) SIFT: predicting amino acid changes that affect protein function. *Nucleic Acids Res* 31: 3812–3814.
24. Yuan JS, Reed A, Chen F, Stewart CN Jr. (2006) Statistical analysis of real-time PCR data. *BMC Bioinformatics* 7: 85–96.
25. Bonora E, Evangelisti C, Bonichon F, Tallini G, Romeo G. (2006) Novel germline variants identified in the inner mitochondrial membrane transporter TIMM44 and their role in predisposition to oncocytic thyroid carcinomas. *Br J Cancer* 95: 1529–1536.
26. Máximo V, Botelho T, Capela J, Soares P, Lima J, et al. (2005) Somatic and germline mutation in GRIM-19, a dual function gene involved in mitochondrial metabolism and cell death, is linked to mitochondrion-rich (Hurthle cell) tumours of the thyroid. *Br J Cancer* 92: 1892–1898.
27. Porra V, Ferraro-Peyret C, Durand C, Selmi-Ruby S, Giroud H, et al. (2005) Silencing of the tumor suppressor gene SLC5A8 is associated with BRAF mutations in classical papillary thyroid carcinomas. *J Clin Endocrinol Metab* 90: 3028–3035.
28. Sekhar KR, Yan XX, Freeman ML. (2002) Nrf2 degradation by the ubiquitin proteasome pathway is inhibited by KIAA0132, the human homolog to INrf2. *Oncogene* 21: 6829–6834.
29. McMahon M, Itoh K, Yamamoto M, Hayes JD. (2003) Keap1-dependent proteasomal degradation of transcription factor Nrf2 contributes to the negative regulation of antioxidant response element-driven gene expression. *J Biol Chem* 278: 21592–21600.
30. Kobayashi A, Kang MI, Okawa H, Ohtsuji M, Zenke Y, et al. (2004) Oxidative stress sensor Keap1 functions as an adaptor for Cul3-based E3 ligase to regulate proteasomal degradation of Nrf2. *Mol Cell Biol* 24: 7130–7139.
31. Shibata T, Kokubo A, Gotoh M, Ojima H, Ohata T, et al. (2008) Genetic alteration of Keap1 confers constitutive Nrf2 activation and resistance to chemotherapy in gallbladder cancer. *Gastroenterology* 135: 1358–1368.
32. Taguchi K, Motohashi H, Yamamoto M. (2011) Molecular mechanisms of the Keap1–Nrf2 pathway in stress response and cancer evolution. *Genes Cells* 16: 123–140.
33. Hayes JD, McMahon M. (2009) NRF2 and KEAP1 mutations: permanent activation of an adaptive response in cancer. *Trends Biochem Sci* 34: 176–188.
34. DeNicola GM, Karreth FA, Humpton TJ, Gopinathan A, Wei C, et al. (2011) Oncogene-induced Nrf2 transcription promotes ROS detoxification and tumorigenesis. *Nature* 475: 106–109.